First-principles Demonstration of Diffusive-advective Particle Acceleration in Kinetic Simulations of Relativistic Plasma Turbulence

Kai Wong[1], Vladimir Zhdankin[2,5], Dmitri A. Uzdensky[1], Gregory R. Werner[1] , and Mitchell C. Begelman[3,4]

[1] Center for Integrated Plasma Studies, Physics Department, 390 UCB, University of Colorado, Boulder, CO 80309, USA
[2] Department of Astrophysical Sciences, Princeton University, Peyton Hall, Princeton, NJ 08544, USA
[3] JILA, University of Colorado and National Institute of Standards and Technology, 440 UCB, Boulder, CO 80309, USA
[4] Department of Astrophysical and Planetary Sciences, 391 UCB, Boulder, CO 80309, USA

Abstract

Nonthermal relativistic plasmas are ubiquitous in astrophysical systems like pulsar wind nebulae and active galactic nuclei, as inferred from their emission spectra. The underlying nonthermal particle acceleration (NTPA) processes have traditionally been modeled with a Fokker–Planck (FP) diffusion-advection equation in momentum space. In this Letter, we directly test the FP framework in ab initio kinetic simulations of driven magnetized turbulence in relativistic pair plasma. By statistically analyzing the motion of tracked particles, we demonstrate the diffusive nature of NTPA and measure the FP energy diffusion (D) and advection (A) coefficients as functions of particle energy $\gamma m_e c^2$. We find that $D(\gamma)$ scales as γ^2 in the high-energy nonthermal tail, in line with second-order Fermi acceleration theory, but has a much weaker scaling at lower energies. We also find that A is not negligible and reduces NTPA by tending to pull particles toward the peak of the particle energy distribution. This study provides strong support for the FP picture of turbulent NTPA, thereby enhancing our understanding of space and astrophysical plasmas.

Unified Astronomy Thesaurus concepts: High energy astrophysics (739); Non-thermal radiation sources (1119); Plasma astrophysics (1261)

1. Introduction

Relativistic plasmas with nonthermal power-law energy distributions are ubiquitous in astrophysical systems such as pulsar wind nebulae (PWN; Meyer et al. 2010; Bühler & Blandford 2014), jets from active galactic nuclei (AGNs; Begelman et al. 1984; Hartman et al. 1992) and their radio lobes (Hardcastle et al. 2009), and black hole accretion-disk coronae (Yuan et al. 2003). The underlying nonthermal particle acceleration (NTPA) processes have been studied theoretically for decades; proposed mechanisms include collisionless shocks (Blandford & Eichler 1987), turbulence (Kulsrud & Ferrari 1971), and magnetic reconnection (Hoshino & Lyubarsky 2012). The most common turbulent NTPA models posit that particles gain energy in a stochastic process (e.g., scattering off of magnetic fluctuations) that can be modeled using Fokker–Planck (FP) advection-diffusion equation in momentum space (Fermi 1949; Kulsrud & Ferrari 1971; Melrose 1974; Skilling 1975; Blandford & Eichler 1987; Schlickeiser 1989; Miller et al. 1990; Chandran 2000; Cho & Lazarian 2006).

Numerical tests of the FP framework for NTPA were originally performed by injecting test particles into magnetohydrodynamic simulations (Dmitruk et al. 2003, 2004; Kowal et al. 2012; Lynn et al. 2014; Kimura et al. 2016; Isliker et al. 2017b) or artificially prescribed fields (Arzner et al. 2006; O'Sullivan et al. 2009). These test-particle simulations are relatively inexpensive, but have physical limitations such as ad hoc particle injection and the absence of particle feedback on the fields, which can only be resolved by considering more physically complete simulations.

Recently, first-principles kinetic (and hybrid) particle-in-cell (PIC) simulations have confirmed that turbulence (Kunz et al. 2016; Makwana et al. 2017; Zhdankin et al. 2017, 2018b, 2019; Comisso & Sironi 2018; Arzamasskiy et al. 2019), shocks (Hoshino et al. 1992; Amato & Arons 2006; Spitkovsky 2008; Sironi & Spitkovsky 2011; Marcowith et al. 2016), and relativistic reconnection (Zenitani & Hoshino 2001; Jaroschek et al. 2004; Lyubarsky & Liverts 2008; Guo et al. 2014, 2016; Sironi & Spitkovsky 2014; Werner et al. 2016, 2018; Werner & Uzdensky 2017) can generate efficient NTPA in collisionless plasma. PIC simulations contain complete microphysical information including the self-consistent trajectories and energy histories of individual particles. However, this wealth of data has not yet been employed directly to test stochastic acceleration models (e.g., FP) or to measure the energy diffusion and advection coefficients.

In this Letter, we use tracked particles to demonstrate stochastic acceleration and directly measure the FP coefficients in three-dimensional (3D) PIC simulations of driven turbulence in collisionless relativistic plasma. Stochastic particle acceleration in relativistic plasma turbulence has important applications to astrophysical systems such as PWN (Bucciantini et al. 2011; Tanaka & Asano 2017), AGN accretion flows (Dermer et al. 1996; Kimura et al. 2015), AGN jets (Rieger et al. 2007; Asano et al. 2014), and gamma-ray bursts (Dermer & Humi 2001). We consider pair plasma both for theoretical and computational simplicity, and for its relevance to high-energy astrophysical systems like PWN and AGN jets. However, our methods also apply to future investigations of NTPA in turbulent non-relativistic and electron-ion plasmas, as well as to other processes, e.g., magnetic reconnection.

---

[5] NASA Einstein fellow.

2. Method

We analyze 3D simulations (performed with our PIC code ZELTRON Cerutti et al. 2013) of externally driven turbulence in relativistic pair plasma (Zhdankin et al. 2018b). We focus on the largest simulation with 1563^3 grid cells and 64 particles per cell (electrons and positrons combined), totaling $\sim 2.4 \times 10^{11}$ particles; smaller simulations give similar results. The simulation domain is a periodic cube of size L, with an initially uniform magnetic guide field $B_0\hat{z}$. The plasma is initially uniform and isotropic, with total charged particle density n_0, and a Maxwell–Jüttner thermal distribution with a relativistically hot temperature of $T_0 = 100 m_e c^2$, corresponding to the average Lorentz factor $\overline{\gamma}_{\rm init} \approx 3T_0/m_e c^2 = 300$. The initial magnetization is $\sigma_0 = B_0^2/16\pi n_0 T_0 = 3/8$. In the fiducial simulation, the normalized system size is $L/2\pi\rho_{e0} = 163$, where $\rho_{e0} \equiv \overline{\gamma}_{\rm init} m_e c^2/eB_0$ is the initial characteristic Larmor radius. Turbulence is electromagnetically driven (TenBarge et al. 2014) and becomes fully developed after several light-crossing times (Zhdankin et al. 2018a), with rms turbulent magnetic fluctuations $\delta B_{\rm rms} \sim B_0$. The turbulence is essentially Alfvénic (Zhdankin et al. 2018a), with initial Alfvén velocity $v_{A0}/c \equiv [\sigma_0/(\sigma_0 + 1)]^{1/2} \simeq 0.52$.

Our previous studies (Zhdankin et al. 2017, 2018b) have shown that such turbulence reliably produces nonthermal power-law particle spectra. In this section, we describe our procedure to investigate NTPA in relation to the FP framework. First, we examine gyro-scale oscillations in particle energy and explain their physical origin. Then, we present our methodology for averaging out these oscillations, which is critical for accurately measuring energy diffusion. Finally, we detail our tests of diffusive NTPA in our turbulence simulations, and our procedure for measuring the energy diffusion and advection coefficients as functions of particle energy.

Our analysis tracks the positions, momenta, and local electromagnetic field vectors for a statistical ensemble of 8×10^5 randomly chosen particles. We observe order-unity oscillations in particle energy, $\gamma m_e c^2$, at the gyrofrequency, as shown for a representative particle in Figure 1(a). The energy oscillates once per gyro-orbit (Figure 1(b)) because of the large-scale electric field accelerating and decelerating the particle as it gyrates. To describe this analytically, we consider a charged particle moving in constant, uniform electromagnetic fields. We use primed variables for the frame moving with the $\boldsymbol{E} \times \boldsymbol{B}$ drift velocity, $\boldsymbol{v}_D$, given by $c\boldsymbol{v}_D/(c^2 + v_D^2) = \boldsymbol{E} \times \boldsymbol{B}/(E^2 + B^2)$.

In the primed frame, where $\boldsymbol{B}'$ and $\boldsymbol{E}'$ are parallel, the particle gyrates about $\boldsymbol{B}'$ while being accelerated along $\boldsymbol{B}'$ by $\boldsymbol{E}'$. Typically, $E' \ll B'$, and so $\gamma' m_e c^2$ is slowly varying on the oscillation timescale. Then, the motion in the primed frame is approximately a simple gyration with $\boldsymbol{E}' \approx 0$, and, applying the inverse Lorentz transformation, the lab-frame energy can be found:

$$\gamma(t) = \gamma_D \gamma' \left(1 + \beta_D \frac{v_\perp'}{c} \cos\omega' t'\right), \quad (1)$$

with $t = t_0 + \gamma_D(t' + \beta_D v_\perp' \sin\omega' t'/\omega' c)$. Here, t is the coordinate time, $v_\perp'$ is the particle's primed-frame velocity perpendicular to $\boldsymbol{B}'$, $\beta_D = v_D/c$, $\gamma_D = (1 - v_D^2/c^2)^{-1/2}$, $\omega' = eB'/\gamma' m_e c$ is the cyclotron frequency with $B' = B/\gamma_D$, and t_0 is a phase. Since we are considering relativistic particles ($v_\perp' \sim c$) and relativistic turbulence ($E_{\rm rms} \sim B_0$ and $\beta_D \sim 1$),
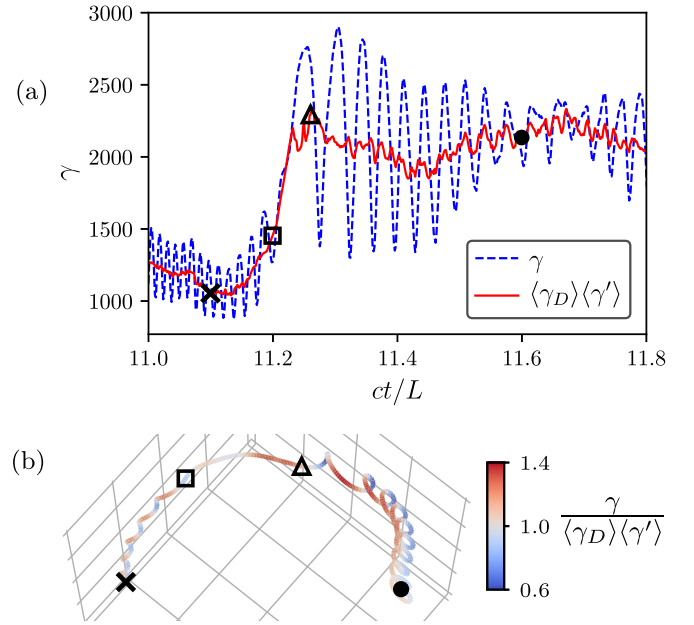

Figure 1. (a) Partial energy history of a tracked particle (blue dashed line), showing oscillations that are removed by our transformation (red solid line). (b) Trajectory of the same particle, colored by the instantaneous ratio of the lab-frame energy to the smoothed energy. Markers show time instances in (a) corresponding to particle positions in (b).

the predicted oscillation magnitude is comparable to γ (see Figure 1(a)), and cannot be ignored.

Without further processing, these energy oscillations are incompatible with a random-walk-based energy-diffusion model. However, we aim to measure the statistical properties of NTPA on the Alfvénic timescale $\sim L/v_A$ relevant to the formation of the nonthermal power law. Since this is generally much longer than the gyroperiod, we analyze just the secular component of the energy histories.

Our oscillation removal procedure is informed by Equation (1), which indicates that in the idealized case of uniform constant fields, the secular component of the lab-frame energy is $\gamma_D \gamma'$. However, $\boldsymbol{v}_D$ fluctuates as the particle traverses small-scale fields, so we average $\boldsymbol{v}_D$ over the smoothed gyroperiod $2\pi\gamma' m_e c/eB$, where $\gamma' = \gamma_D \gamma(1 - \boldsymbol{v}_D \cdot \boldsymbol{v}/c^2)$ is obtained from boosting the lab-frame four-velocity $\gamma\boldsymbol{v}$ by $\boldsymbol{v}_D$. We denote by $\langle\boldsymbol{v}_D\rangle$ the average of $\boldsymbol{v}_D$ over this smoothed period. We then define the smoothed particle energy to be $\langle\gamma_D\rangle\langle\gamma'\rangle$, where $\langle\gamma'\rangle = \langle\gamma_D\rangle\gamma(1 - \langle\boldsymbol{v}_D\rangle \cdot \boldsymbol{v}/c^2)$ and $\langle\gamma_D\rangle \equiv (1 - \langle\boldsymbol{v}_D\rangle^2/c^2)^{-1/2}$. This transformed energy (Figure 1(a)) has greatly reduced oscillations. Thus, this procedure extracts the secular component of particle energy, allowing us to test the FP picture of NTPA. Hereafter, γ and "energy" refer to $\langle\gamma_D\rangle\langle\gamma'\rangle$, except in the case of the overall particle energy distributions (Figure 4(a)) and magnetic energy spectra (Figure 4(b)).

We now describe our tests of diffusive acceleration using tracked particles. We use $t_0 = 10.0L/c$ as a fiducial initial time for our measurements, by which point a power-law particle energy spectrum has fully formed. We then bin tracked particles by their energy at t_0 in logarithmic intervals spaced by 10%. For each bin, we measure the standard deviation, $\delta\gamma_{\rm rms}$, and the mean, $\overline{\gamma}$, of the particle energy distribution as a function of subsequent times $\Delta t \equiv t - t_0$. For a classical diffusion process, one expects $\delta\gamma_{\rm rms}(\Delta t) \propto \sqrt{\Delta t}$ if the
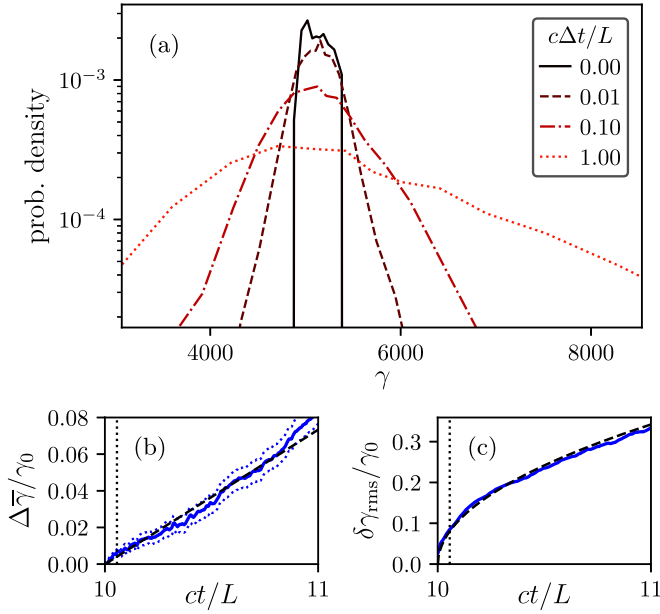
Figure 2. (a) Time evolution of the energy distribution for a bin of $N \sim 2200$ particles with bin-center energy $\gamma_0 = 5 \times 10^3$. For this bin, (b) shows $\overline{\gamma}(t)/\gamma_0$ (solid) with standard error ranges $(\overline{\gamma}(t) \pm \delta\gamma_{\rm rms}(t)/\sqrt{N})/\gamma_0$ (dotted) and a linear Δt fit (dashed), and (c) shows $\delta\gamma_{\rm rms}(t)/\gamma_0$ (solid) with a $\sqrt{\Delta t}$ fit (dashed). In (b) and (c), a vertical dotted line is placed at $\Delta t = T_{\rm L}(\gamma_0, B_{\rm rms})$, the gyroperiod corresponding to γ_0.

diffusion coefficient $D(\gamma, t)$ varies slowly compared with Δt and $\delta\gamma_{\rm rms}$.

We then measure the diffusion and advection coefficients, $D(\gamma)$ and $A(\gamma)$, respectively, for the simplest FP equation for the energy distribution $f(\gamma, t)$, ignoring pitch angle (with respect to $\boldsymbol{B}$):

$$\partial_t f = \partial_\gamma (D \partial_\gamma f) - \partial_\gamma (Af). \tag{2}$$

Limiting our measurements to times where $\Delta t \lesssim L/v_{\rm A}$, $\delta\gamma_{\rm rms} \ll \gamma_0$, and $\Delta\overline{\gamma} \equiv \overline{\gamma}(t) - \overline{\gamma}(t_0) \ll \gamma_0$, we approximate the bin distribution as narrow and the coefficients as constant in time. Applying Equation (2), we find

$$\Delta\overline{\gamma}(\gamma_0, \Delta t) = [\partial_\gamma D|_{\gamma_0} + A(\gamma_0)]\Delta t \equiv M(\gamma_0)\Delta t \tag{3}$$

$$\delta\gamma_{\rm rms}(\gamma_0, \Delta t) = \sqrt{2D(\gamma_0)\Delta t}. \tag{4}$$

We first measure $D(\gamma)$ and $M(\gamma)$ by applying Equations (3) and (4) to each energy bin and then calculate $A(\gamma) \equiv M - \partial_\gamma D$.

3. Results

We first describe the evolution of the overall lab-frame distribution, $f(\gamma)$. Starting from a thermal distribution, $f(\gamma)$ acquires a power-law tail extending to the system-size limit, $\gamma_{\rm max} \equiv LeB_0/2m_e c^2 \simeq 1.5 \times 10^5$, and gradually hardening over time—its index converges to approximately -3 by $12.3L/c$. At the start of our measurements, $t_0 = 10.0L/c$, the index is approximately -3.2, the peak of $f(\gamma)$ is at $\gamma_{\rm peak} \simeq 520$, and the mean at $\gamma_{\rm avg} \simeq 1170$. Because the system lacks an energy sink, $\gamma_{\rm peak}$ and $\gamma_{\rm avg}$ increase at a rate of about $40c/L$ and $100c/L$, respectively.

We now present tests of energy diffusion. For illustration, Figure 2(a) shows the evolution of the energy distribution of a single bin of particles with $\gamma_0 = 5 \times 10^3$, deep in the power-
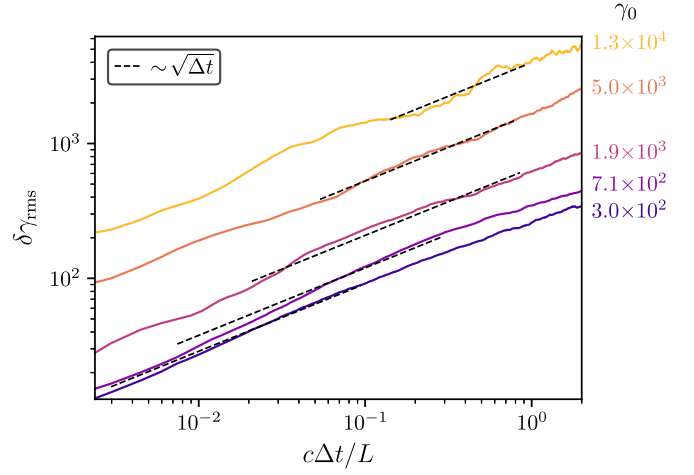

Figure 3. Standard deviation, $\delta\gamma_{\rm rms}$, of the particle energies in several bins (solid lines), with corresponding $\sqrt{\Delta t}$ fits (dashed lines), each annotated by the initial bin-center energy γ_0. Each fit is drawn over the corresponding fitting interval, which begins at $\Delta t = T_{\rm L}(\gamma_0, B_{\rm rms})$, the gyroperiod for the bin-center energy of the corresponding bin.

law section. We find that $\overline{\gamma} \propto \Delta t$ for small Δt (Figure 2(b)), while $\delta\gamma_{\rm rms}(\Delta t) \propto \sqrt{\Delta t}$ (Figure 2(c)), consistent with simple diffusion.

Figure 3 shows $\delta\gamma_{\rm rms}(\Delta t)$ for several bins along with corresponding $\sqrt{\Delta t}$ fits. To avoid artifacts of the smoothing procedure, each fit begins after one gyroperiod $T_{\rm L}(\gamma_0, B_{\rm rms}) \equiv 2\pi\gamma_0 m_e c/eB_{\rm rms}$. To ensure Equations (3) and (4) are valid, each fit ends when $\delta\gamma_{\rm rms}/\gamma_0$ reaches 0.3, $\Delta\overline{\gamma}/\gamma_0$ reaches 0.1, or $\Delta t = 2L/c$, whichever is earliest. Under these criteria, almost all fits end before $\Delta t = 1L/c$. The fits generally agree well with the data over the fitted intervals. While some of the plotted $\delta\gamma_{\rm rms}(\Delta t)$ have intervals of weakly anomalous energy diffusion these regimes are not our current focus, and we refer to studies of anomalous energy diffusion in plasma turbulence (Isliker et al. 2017b, 2017a). In summary, Figures 2 and 3 confirm our expectations of a standard diffusive process, supporting the FP model of turbulent NTPA.

We now report on our measurements of $D(\gamma)$ and $A(\gamma)$. Figure 4(c) shows $D(\gamma)$, extracted from the fits of $\delta\gamma_{\rm rms}(\Delta t)$ using Equation (4). In the high-energy nonthermal tail $(2 \times 10^3 \lesssim \gamma \lesssim 3 \times 10^4$, see Figure 4(a)), $D = 0.06(c/L)\gamma^2$ is an excellent fit, while for lower energies $\gamma \lesssim \gamma_{\rm peak}$, there is a much shallower scaling roughly consistent with $D \propto \gamma^{2/3}$. We observe that $D \propto \gamma^2$ for particles gyroresonant with fluctuations in the inertial range of the magnetic energy spectrum (Figure 4(b)), while the lower-energy scaling corresponds to the sub-inertial range of turbulence. In simulations with different magnetization, system size, and number of particles per cell (not shown), the high-energy scaling of $D \propto \gamma^2$ is maintained while the low-energy behavior varies slightly.

The high-energy scaling of $D \propto \gamma^2$ is commonly predicted by NTPA theories (Kulsrud & Ferrari 1971; Skilling 1975; Blandford & Eichler 1987; Schlickeiser 1989; Chandran 2000; Cho & Lazarian 2006). We compare our high-energy fit, $D/\gamma^2 = 0.06c/L$, to the theoretical prediction from second-order Fermi acceleration, $D/\gamma^2 = u_{\rm A}^2/3c\lambda_{\rm mfp}$, for ultra-relativistic particles interacting with isotropic scatterers moving at the Alfvén velocity, where $u_{\rm A} = v_{\rm A}/(1 - v_{\rm A}^2/c^2)^{1/2}$ and $\lambda_{\rm mfp}$ is the mean free path between scattering events (Blandford &
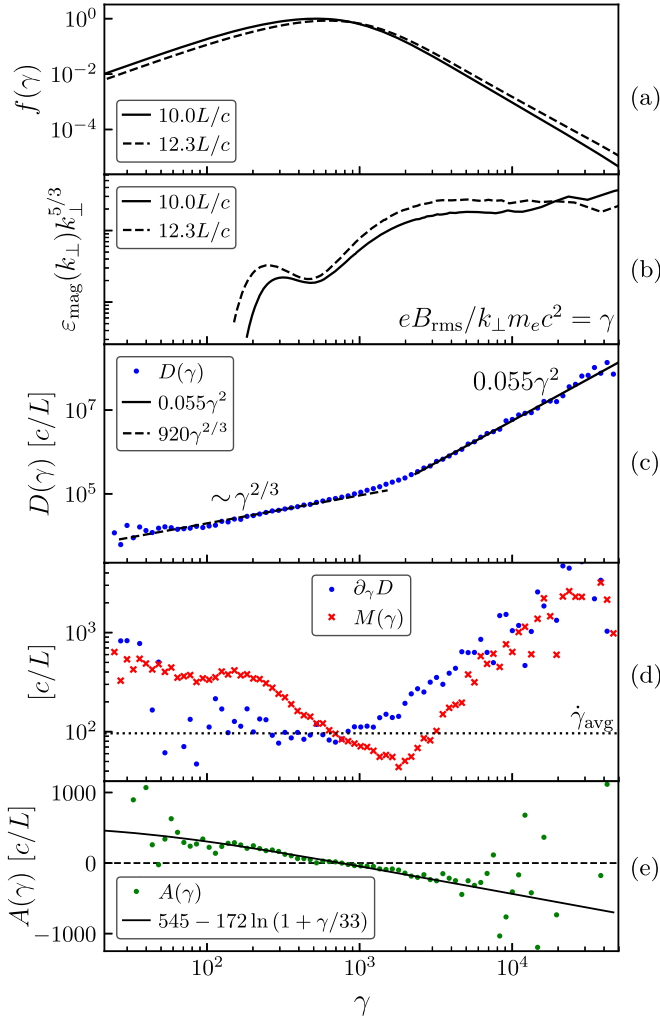
Figure 4. (a) The overall particle energy distribution $f(\gamma)$ at the start of the measuring interval ($t = 10.0L/c$, solid line), and a short time later ($t = 12.3L/c$, dashed line). (b) The magnetic energy spectrum $\epsilon_{\mathrm{mag}}(k_\perp)$ compensated by $k_\perp^{5/3}$ vs. $eB_{\mathrm{rms}}/k_\perp m_e c^2$, the Lorentz factor corresponding to a perpendicular gyroradius equal to the inverse of the perpendicular (to B_0) wavenumber $k_\perp$. (c) The diffusion coefficient $D(\gamma)$ (dots), with power-law fits of index 2 (solid line) in the nonthermal region, and index 2/3 (dashed line) in the low-energy region. (d) The acceleration rate $M(\gamma)$ (crosses) and the contribution to $M(\gamma)$ by $\partial_\gamma D$ (dots). For reference, the overall average rate of energy gain $\dot\gamma_{\mathrm{avg}} \simeq 100c/L$ is shown as a dotted line. (e) The advection coefficient $A(\gamma) \equiv M - \partial_\gamma D$ (dots) with logarithmic fit (solid line).

Eichler 1987; Longair 2011). At $t_0 = 10.0L/c$, $v_A = 0.51c$, giving a theoretical scaling of $D/\gamma^2 = 0.12c/\lambda_{\mathrm{mfp}}$, which agrees with our fit if $\lambda_{\mathrm{mfp}} \sim 2L$. We also find, from simulations with reduced driving wavelength (not shown), that the turbulence driving scale, and not the box size, sets D/γ^2 (and hence λ_{mfp}). While the value of D/γ^2 is consistent with second-order Fermi acceleration from gyroresonant scattering of particles by Alfvén modes, further work is needed to test this view. This includes studying the effect of varying magnetization, as well as the spatial transport characteristics.

To compare the effects of the first- and second-order derivative terms in Equation (2), we separate the contributions of A and $\partial_\gamma D$ to the average acceleration rate $M(\gamma) = \partial_t \overline{\gamma}$. We extract $M(\gamma)$ from linear fits of $\overline{\gamma}(\Delta t)$ (see Equation (3)), using the same time intervals as those used for fitting $\delta\gamma_{\mathrm{rms}}(\Delta t)$ to measure $D(\gamma)$. As shown in Figure 4(d), $M(\gamma)$ is positive, as

expected with external energy injection, and has a minimum near $\gamma_{\mathrm{avg}} \approx 1200$.

We then compute the contribution of energy diffusion to acceleration, $\partial_\gamma D$, (Figure 4(d)) and subsequently the advection coefficient $A(\gamma) \equiv M - \partial_\gamma D$ (Figure 4(e)). In the high-energy power-law section ($\gamma > \gamma_{\mathrm{peak}}$), A is negative, while for low energies ($\gamma < \gamma_{\mathrm{peak}}$), A is positive. Overall, A tends to pull particle energies toward γ_{peak}, narrowing $f(\gamma)$. We find that A is reasonably approximated by a logarithmic scaling with energy. For a momentum-space FP equation containing only diffusion (see, e.g., Ramaty 1979), the expected energy-space advection coefficient for Equation (2) is $A = 2D/\gamma$. The measured negative logarithmic scaling thus implies that the momentum-space FP equation contains a significant advection term. In the nonthermal section, the magnitude of A is generally smaller than, but still comparable to that of $\partial_\gamma D$. Hence, the evolution of the nonthermal population in this simulation cannot be interpreted as being due to D alone. This also complicates estimates of the acceleration time based on D/γ^2. The rate of overall energy increase from advection is $\int d\gamma A f \approx -23c/L$, while that from diffusion is $\int d\gamma (\partial_\gamma D) f \approx 140c/L$. The general effects of systematic and stochastic acceleration (due to A and D, respectively) are discussed in, e.g., Pisokas et al. (2018) and Vlahos & Isliker (2019). We note that our measurement of A has considerable scatter outside of the central range, $10^2 \lesssim \gamma \lesssim 10^4$, as it depends on the difference between two noisy quantities.

Finally, we test whether the FP equation with coefficients measured by our methodology can reproduce the evolution of $f(\gamma, t)$ from the PIC simulations. We first repeat the measurements of D and A at almost 200 different t_0 evenly spaced over the entire simulation, thus obtaining time-dependent coefficients. We then insert the measured coefficients into the FP equation (Equation (2)) and solve it numerically using a finite-volume method. We use linear interpolation in γ and nearest-neighbor interpolation in t. The FP coefficients are extrapolated as constant in γ for energies without enough particles to measure them. Comparing with the particle energy distributions obtained from the PIC simulation, we find that the FP equation gives excellent agreement at all subsequent times when initialized with the corresponding PIC distribution as early as $t = 4.5L/c$ (Figure 5(a)), with moderate errors if initialized at $t = 0$ (Figure 5(b)). This may be due to the turbulence not being fully developed at early times. Finally, evolving from $t = 4.5L/c$ with A set to zero shows a clear mismatch with the PIC distributions (Figure 5(c)), giving us confidence that the measurements of A are reasonably accurate and that A significantly affects the evolution of $f(\gamma, t)$. Thus, in this regime of fully developed turbulence, we find that the FP equation with our coefficient measurement methodology is appropriate for modeling NTPA. We leave further investigation of the early-time behavior to future work.

4. Conclusions

In this study we rigorously demonstrate, for the first time, diffusive NTPA in first-principles PIC simulations of driven relativistic plasma turbulence, through direct statistical measurements using large numbers of tracked particles. We introduce a procedure to suppress large-amplitude gyro-oscillations of particle energy, which is critical for revealing the diffusive nature of NTPA and measuring the FP
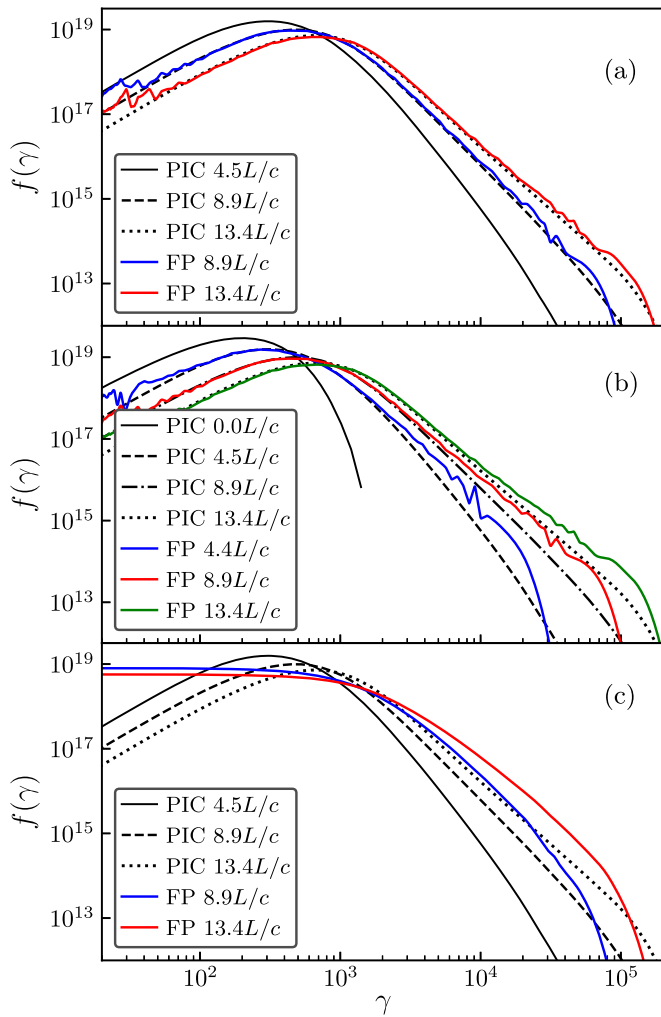
Figure 5. (a) Particle distributions $f(\gamma)$ from the PIC simulation at $ct/L \in \{4.5, 8.9, 13.4\}$ (black solid, dashed, and dotted lines, respectively), and the FP solution (initialized at $ct/L = 4.5$) at $ct/L \in \{8.9, 13.4\}$ (red and blue solid lines, respectively). (b) Similar to (a) but for an FP solution initialized at $ct/L = 0$. (c) Similar to (a) but with the advection coefficient artificially set to zero.

coefficients. We find that the energy diffusion coefficient D scales with particle energy $\gamma m_e c^2$ as $D \simeq 0.06(c/L)\gamma^2$ in the high-energy nonthermal power-law region, in line with theoretical expectations (Kulsrud & Ferrari 1971; Skilling 1975; Blandford & Eichler 1987; Schlickeiser 1989; Chandran 2000; Cho & Lazarian 2006), while there is a much shallower scaling at energies below the peak of the energy distribution. We also measure the energy advection coefficient $A(\gamma)$, though with more uncertainty. We find that A is not negligible, and tends to narrow the distribution by accelerating low-energy particles and decelerating high-energy particles. Furthermore, a numerical solution of the FP equation with the measured coefficients reproduces the evolution of the particle energy spectrum from the PIC simulation over a significantly longer time interval than was used for measuring the coefficients. This suggests that this simple FP model can fully account for NTPA in our simulations. These results thus lend strong first-principles numerical support to a broad class of turbulent NTPA theories.

Our new methodology can also be applied to future tracked-particle studies of NTPA in other contexts such as shocks or magnetic reconnection, and over broader ranges of physical

regimes. Future work may investigate the effects of system parameters such as magnetization, plasma beta, and guide field strength; radiative cooling; relativistic versus non-relativistic regimes; and plasma composition (e.g., pair versus electron-ion plasma). In addition, the analysis can be extended to include pitch-angle dependence and scattering. Characterizing stochastic NTPA in various regimes has important implications in a broad range of contexts such as solar flares, the solar wind, PWN, AGNs, gamma-ray bursts, and cosmic-ray acceleration in supernova remnants. Thus, this study will facilitate more detailed tests of NTPA theories against PIC simulations exploring various physical situations, thereby advancing our understanding of space, solar, and high-energy astrophysical phenomena.

ORCID iDs

Gregory R. Werner ● https://orcid.org/0000-0001-9039-9032
Mitchell C. Begelman ● https://orcid.org/0000-0003-0936-8488

References

Amato, E., & Arons, J. 2006, ApJ, 653, 325
Arzamasskiy, L., Kunz, M. W., Chandran, B. D. G., & Quataert, E. 2019, ApJ, 879, 53
Arzner, K., Knaepen, B., Carati, D., Denewet, N., & Vlahos, L. 2006, ApJ, 637, 322
Asano, K., Takahara, F., Kusunose, M., Toma, K., & Kakuwa, J. 2014, ApJ, 780, 64
Begelman, M. C., Blandford, R. D., & Rees, M. J. 1984, RvMP, 56, 255
Blandford, R., & Eichler, D. 1987, PhR, 154, 1
Bucciantini, N., Arons, J., & Amato, E. 2011, MNRAS, 410, 381
Bühler, R., & Blandford, R. 2014, RPPh, 77, 066901
Cerutti, B., Werner, G. R., Uzdensky, D. A., & Begelman, M. C. 2013, ApJ, 770, 147
Chandran, B. D. G. 2000, PhRvL, 85, 4656
Cho, J., & Lazarian, A. 2006, ApJ, 638, 811
Comisso, L., & Sironi, L. 2018, PhRvL, 121, 255101
Dermer, C. D., & Humi, M. 2001, ApJ, 556, 479
Dermer, C. D., Miller, J. A., & Li, H. 1996, ApJ, 456, 106
Dmitruk, P., Matthaeus, W. H., & Seenu, N. 2004, ApJ, 617, 667
Dmitruk, P., Matthaeus, W. H., Seenu, N., & Brown, M. R. 2003, ApJL, 597, L81
Fermi, E. 1949, PhRv, 75, 1169
Guo, F., Li, H., Daughton, W., & Liu, Y.-H. 2014, PhRvL, 113, 155005
Guo, F., Li, X., Li, H., et al. 2016, ApJL, 818, L9
Hardcastle, M. J., Cheung, C. C., Feain, I. J., & Stawarz, Ł. 2009, MNRAS, 393, 1041
Hartman, R. C., Bertsch, D. L., Fichtel, C. E., et al. 1992, ApJL, 385, L1
Hoshino, M., Arons, J., Gallant, Y. A., & Langdon, A. B. 1992, ApJ, 390, 454
Hoshino, M., & Lyubarsky, Y. 2012, SSRv, 173, 521
Isliker, H., Pisokas, T., Vlahos, L., & Anastasiadis, A. 2017a, ApJ, 849, 35
Isliker, H., Vlahos, L., & Constantinescu, D. 2017b, PhRvL, 119, 045101
Jaroschek, C. H., Lesch, H., & Treumann, R. A. 2004, ApJL, 605, L9
Kimura, S. S., Murase, K., & Toma, K. 2015, ApJ, 806, 159
Kimura, S. S., Toma, K., Suzuki, T. K., & Inutsuka, S.-i. 2016, ApJ, 822, 88
Kowal, G., de Gouveia Dal Pino, E. M., & Lazarian, A. 2012, PhRvL, 108, 241102
Kulsrud, R. M., & Ferrari, A. 1971, Ap&SS, 12, 302
Kunz, M. W., Stone, J. M., & Quataert, E. 2016, PhRvL, 117, 235101

Longair, M. S. 2011, High Energy Astrophysics (Cambridge: Cambridge Univ. Press), 564

Lynn, J. W., Quataert, E., Chandran, B. D. G., & Parrish, I. J. 2014, ApJ, 791, 71

Lyubarsky, Y., & Liverts, M. 2008, ApJ, 682, 1436

Makwana, K., Li, H., Guo, F., & Li, X. 2017, JPhCS, 837, 012004

Marcowith, A., Bret, A., Bykov, A., et al. 2016, RPPh, 79, 046901

Melrose, D. B. 1974, SoPh, 37, 353

Meyer, M., Horns, D., & Zechlin, H.-S. 2010, A&A, 523, A2

Miller, J. A., Guessoum, N., & Ramaty, R. 1990, ApJ, 361, 701

O'Sullivan, S., Reville, B., & Taylor, A. M. 2009, MNRAS, 400, 248

Pisokas, T., Vlahos, L., & Isliker, H. 2018, ApJ, 852, 64

Ramaty, R. 1979, in AIP Conf. Ser. 56, Particle Acceleration Mechanisms in Astrophysics, ed. J. Arons, C. McKee, & C. Max (Melville, NY: AIP), 135

Rieger, F. M., Bosch-Ramon, V., & Duffy, P. 2007, Ap&SS, 309, 119

Schlickeiser, R. 1989, ApJ, 336, 243

Sironi, L., & Spitkovsky, A. 2011, ApJ, 726, 75

Sironi, L., & Spitkovsky, A. 2014, ApJL, 783, L21

Skilling, J. 1975, MNRAS, 172, 557

Spitkovsky, A. 2008, ApJL, 682, L5

Tanaka, S. J., & Asano, K. 2017, ApJ, 841, 78

TenBarge, J. M., Howes, G. G., Dorland, W., & Hammett, G. W. 2014, CoPhC, 185, 578

Vlahos, L., & Isliker, H. 2019, PPCF, 61, 014020

Werner, G. R., & Uzdensky, D. A. 2017, ApJL, 843, L27

Werner, G. R., Uzdensky, D. A., Begelman, M. C., Cerutti, B., & Nalewajko, K. 2018, MNRAS, 473, 4840

Werner, G. R., Uzdensky, D. A., Cerutti, B., Nalewajko, K., & Begelman, M. C. 2016, ApJL, 816, L8

Yuan, F., Quataert, E., & Narayan, R. 2003, ApJ, 598, 301

Zenitani, S., & Hoshino, M. 2001, ApJL, 562, L63

Zhdankin, V., Uzdensky, D. A., Werner, G. R., & Begelman, M. C. 2018a, MNRAS, 474, 2514

Zhdankin, V., Uzdensky, D. A., Werner, G. R., & Begelman, M. C. 2018b, ApJL, 867, L18

Zhdankin, V., Uzdensky, D. A., Werner, G. R., & Begelman, M. C. 2019, PhRvL, 122, 055101

Zhdankin, V., Werner, G. R., Uzdensky, D. A., & Begelman, M. C. 2017, PhRvL, 118, 055103